nrap

National Risk
Assessment Partnership

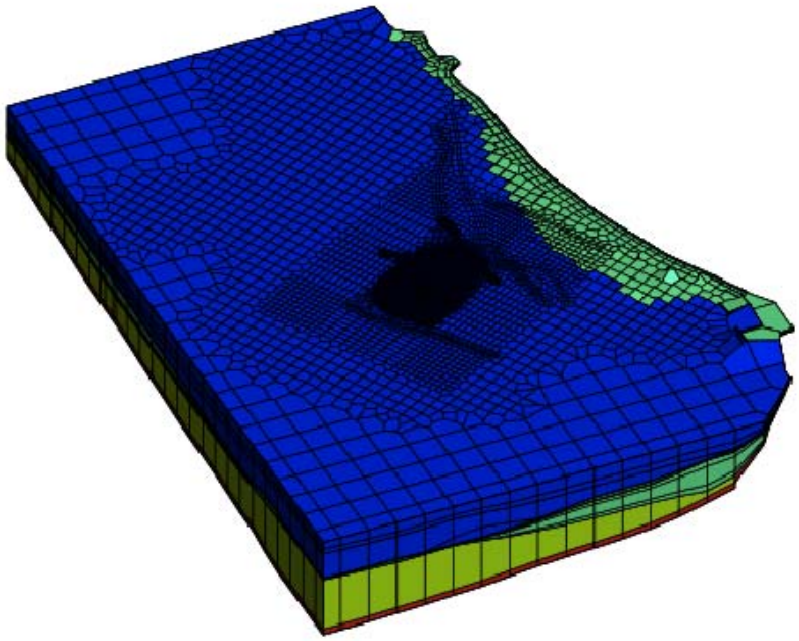

Modeling the Performance of Large-Scale CO_2 Storage Systems: A Comparison of Different Sensitivity Analysis Methods

24 October 2012

U.S. DEPARTMENT OF ENERGY

NETL

Office of Fossil Energy

NRAP-TRS-III-002-2012

Disclaimer

This report was prepared as an account of work sponsored by an agency of the United States Government. Neither the United States Government nor any agency thereof, nor any of their employees, makes any warranty, express or implied, or assumes any legal liability or responsibility for the accuracy, completeness, or usefulness of any information, apparatus, product, or process disclosed, or represents that its use would not infringe privately owned rights. Reference therein to any specific commercial product, process, or service by trade name, trademark, manufacturer, or otherwise does not necessarily constitute or imply its endorsement, recommendation, or favoring by the United States Government or any agency thereof. The views and opinions of authors expressed therein do not necessarily state or reflect those of the United States Government or any agency thereof.

Cover Illustration: A 3D geological model and discretization used in this study.

Suggested Citation: Wainwright, H.; Finsterle, S.; Zhou, Q.; Birkholzer, J. *Modeling the Performance of Large-Scale CO_2 Storage Systems: A Comparison of Different Sensitivity Analysis Methods*; NRAP-TRS-III-002-2012; NRAP Technical Report Series; U.S. Department of Energy, National Energy Technology Laboratory: Morgantown, WV, 2012; p 24.

An electronic version of this report can be found at: www.netl.doe.gov/nrap.

Modeling the Performance of Large-Scale CO_2 Storage Systems: A Comparison of Different Sensitivity Analysis Methods

Haruko Wainwright[1], Stefan Finsterle[1], Quanlin Zhou[1], and Jens Birkholzer[1]

[1]Earth Sciences Division, Lawrence Berkeley National Laboratory, 1 Cyclotron Road Berkeley, CA 94720

NRAP-TRS-III-002-2012

Level III Technical Report Series

24 October 2012

This page intentionally left blank

Table of Contents

1. INTRODUCTION 1

2. MODEL SET UP 3

3. SENSITIVITY ANALYSIS METHODS AND IMPLEMENTATION 5
3.1 LOCAL SENSITIVITY METHOD 5
3.2 MORRIS SENSITIVITY METHOD 5
3.3 SALTELLI SENSITIVITY METHOD 5
3.4 IMPLEMENTATION IN ITOUGH2 6

4. PARAMETER DISTRIBUTION 7

5. RESULTS 9
5.1 BASE-CASE SIMULATION 9
5.2 UNCERTAINTY ANALYSIS 10
5.3 LOCAL SENSITIVITY 11
5.4 MORRIS SENSITIVITY 12
5.5 SALTELLI SENSITIVITY 14

6. DISCUSSION AND CONCLUSION 15
6.1 COMPARISON OF THREE SENSITIVITY METHODS 15
6.2 IMPLICATIONS FOR THE CO_2 STORAGE SYSTEM 15

7. REFERENCES 17

List of Figures

Figure 1: (a) Plan view of the Vedder formation and the faults (the major faults are shown in red.), and (b) Plan view of the numerical domain with mesh. The blue dot is the injection location, and the red dots (Point A and B) are used as points of interest in this study. 3

Figure 2: Estimated depth-dependent (a) V Sand permeability (natural logarithm), and (b) V Sand porosity. The blue dots are the data values, the solid red line is the estimated value, and the dotted red lines are ± two standard deviations.....7

Figure 3: Evolution of pressure buildup (top row; ΔP in MPa) and CO_2 saturation (bottom row) at 20, 50, 100 and 200 yr (left to right columns). The solid thick black lines are fault locations. The thin black lines in the pressure buildup plots represent the 0.2 MPa-contour line. 9

Figure 4: Time profile of the performance measures for the reference parameter case: (a) CO_2 saturation (S_{CO2}), (b) pressure buildup (ΔP), and (c) overpressure zone. 10

Figure 5: Monte-Carlo simulation results; time profiles of the performance measures: (a) CO_2 saturation (S_{CO2}), (b) pressure buildup (ΔP), and (c) overpressure zone. The red line is the mean at each time slice.....10

Figure 6: Local sensitivity results. (a) CO_2 saturation at Point A, (b) pressure buildup at Point B, and (c) overpressure zone. Six most significant parameters are colored and labeled. 11

Figure 7: Morris sensitivity results. (a) CO_2 saturation at Point A, (b) pressure buildup at Point B, and (c) overpressure zone. Six most significant parameters are colored and labeled. 13

Figure 8: Morris sensitivity results. Mean EE vs. STD: (a) CO_2 saturation at Point A, (b) pressure buildup at Point B, and (c) overpressure zone. Six most significant parameters are colored and labeled.....13

Figure 9: Saltelli sensitivity results (a) CO_2 saturation at Point A, (b) Pressure buildup at Point B, and (c) Overpressure extent. 14

List of Tables

Table 1: Reference parameter values: horizontal permeability k_h, anisotropy ratio k_v/k_h, porosity Φ, pore compressibility β_p, van Genuchten α and m. 7

Table 2: Trend parameters for V Sand log-permeability and porosity 8

Acronyms and Abbreviations

Term	Description
EE	Elementary effect
GS	Geologic storage
NRAP	National Risk Assessment Partnership
OAT	One-at-a-time
SA	Sensitivity analysis
STD	Standard deviation
SEM	Standard error of mean
TF Shale	Temblor-Freeman Shale
UA	Uncertainty analysis
UQ	Uncertainty quantification
V Sand	Vedder Sand
V Shale	Vedder Shale

Acknowledgments

This work was completed as part of National Risk Assessment Partnership (NRAP) project. Support for this project came from the DOE Office of Fossil Energy's Crosscutting Research program. The authors wish to acknowledge Robert Romanosky (NETL Strategic Center for Coal) and Regis Conrad (DOE Office of Fossil Energy) for programmatic guidance, direction, and support.

NRAP funding was provided to Lawrence Berkeley National Laboratory (LBNL) under U.S. Department of Energy Contract No. DE-AC02-05CH11231. The authors wish to thank Jeff Wagoner for developing the geologic framework model of the Southern San Joaquin Basin and technical review by Yingqi Zhang (LBNL). Their effort is greatly appreciated.

1. INTRODUCTION

Geologic storage (GS) of CO_2 has been considered as a viable option to reduce CO_2 emissions to the atmosphere. There are various concerns about potential risks associated with injecting large amounts of CO_2 into the deep subsurface, including potential brine/CO_2 leakage and induced seismicity. In order to achieve industrial-scale CO_2 storage, it is important to develop a modeling framework for assessing such risks and selecting the sites with acceptably low risks.

Since system-level modeling of GS risks requires evaluating the entire subsurface storage system (e.g., the target reservoir, the leakage pathways and the potential receptors such as shallow groundwater resources), the use of an integrated multi-scale physics-based model for the entire system would be too computationally demanding to conduct uncertainty quantification over a large range in a high-dimensional parameter space. The current option in the National Risk Assessment Partnership (NRAP) for system-level analysis is therefore to decouple reservoir, leakage, and shallow aquifer simulations. The reservoir-model component plays a key role in such a framework. The reservoir simulations provide various quantities for subsequent analyses; for example, such simulations predict the pressures and CO_2 saturations necessary for computing the leakage risks.

The challenge is that reservoir models often have a large computational mesh and need to solve for complex non-linear processes, such as thermodynamic and thermophysical behavior of H_2O-NaCl-CO_2 mixtures and related phase transitions (Pruess, 2005). Modeling the pressure response to CO_2 injection requires a large domain, since the pressure propagates much farther than the CO_2 plume and is likely to propagate beyond the storage reservoir through the caprock and possibly into overlying formations (Zhou and Birkholzer, 2011). Running such reservoir models multiple times—which is necessary for probabilistic risk assessments—is computationally intensive, and in some cases could make such risk assessments impossible to conduct for exhaustive sets of all the parameters.

Uncertainty quantification (UQ) study, including sensitivity analysis (SA) and uncertainty analysis (UA), is essential in risk assessments. In this context, SA is critical to select important parameters and/or to reduce the number of parameters to be perturbed. SAs can also serve as a basis for developing reduced-order models (Pau et al., 2012). Birkholzer et al. (2011) studied the sensitivity of brine pressurization using a basin-scale reservoir model, which identified important parameters for the regional pressure buildup and dependence of sensitivity on time and measurement locations.

There are several sensitivity methods available: local sensitivity, Morris sensitivity, and Saltelli sensitivity (Sobol index) methods (Morris, 1991; Cacuci, 2003; Saltelli, 2008). The last two methods are called global sensitivity methods, which can provide more robust sensitivity measures with respect to the nonlinearity in system responses and interactions among parameters. The global methods, however, are based on sampling parameters. As a result, they could be computationally intensive. There is also an argument that local sensitivity analysis is sufficient, and that global sensitivity methods do not provide enough additional information to justify investing in large computational resources. This could also be because the use of SA is often limited to ranking the parameter importance without looking at various features such as nonlinearity and interactions.

This work presents a UQ study on reservoir processes during and after CO_2 sequestration, using a high-resolution basin-scale reservoir model. There are three main focuses: (1) to show the feasibility of conducting local and global sensitivity analysis using a high-resolution basin-scale model, (2) to compare different sensitivity measures with respect to interpretation and computational requirements, and (3) to demonstrate the usefulness of SA beyond just ranking the parameter importance.

The reservoir model is based on an earlier modeling study described in by Zhou and Birkholzer (2011), which was conducted for a hypothetical industrial-scale storage project in the Southern San Joaquin Basin in California. The geological structure and hydrogeological parameters of various subsurface layers were determined from field data originally assembled for a planned CO_2 pilot project in the area. The massively parallel version of TOUGH2 was used to simulate CO_2/brine migration and pressure buildup within the CO_2 storage formation and overlying/underlying formations. The model provided a unique opportunity to investigate the impact of hydrogeological parameters and their uncertainty on various performance measures of the CO_2 storage system in a realistic setting.

2. MODEL SET UP

The reservoir-scale CO_2 migration model was developed based on a geological study in the Southern San Joaquin Basin, California, using the geologic and hydrogeologic data obtained from many oil fields in that region (Birkholzer et al., 2011; Zhou et al., 2011; Zhou and Birkholzer, 2011). The domain shown includes twelve discontinuous or continuous (stacked) formations, extending 84 km in the eastern direction and 112 km in the northern direction. The domain also includes several faults, which are considered to be semi-impermeable sealing faults at large depth.

The Vedder formation, considered as the a viable storage option in this region, is a large permeable sandstone formation that dips upward towards a shallow outcrop area located along the eastern model boundary, at an average slope of seven degrees. The overlying Temblor-Freeman Shale (TF Shale) is a suitable caprock formation for stratigraphic containment of the injected supercritical CO_2. Within the Vedder, one may distinguish six alternating sand/shale layers—Vedder Sand (V Sand) and Vedder Shale (V Shale)—based on the well logs. These internal facies are considered laterally continuous in this study. At the (assumed) injection site in the center of the domain, the Vedder formation is 400 m thick, and its top elevation is about 2,750 m below ground surface. The caprock (TF Shale) is about 200 m thick. The areal extent of the Vedder formation is shown in green color in Figure 1(a). The formation pinches out to the far south, west, and north of the injection site, and, as mentioned above, reaches the surface along the eastern boundary.

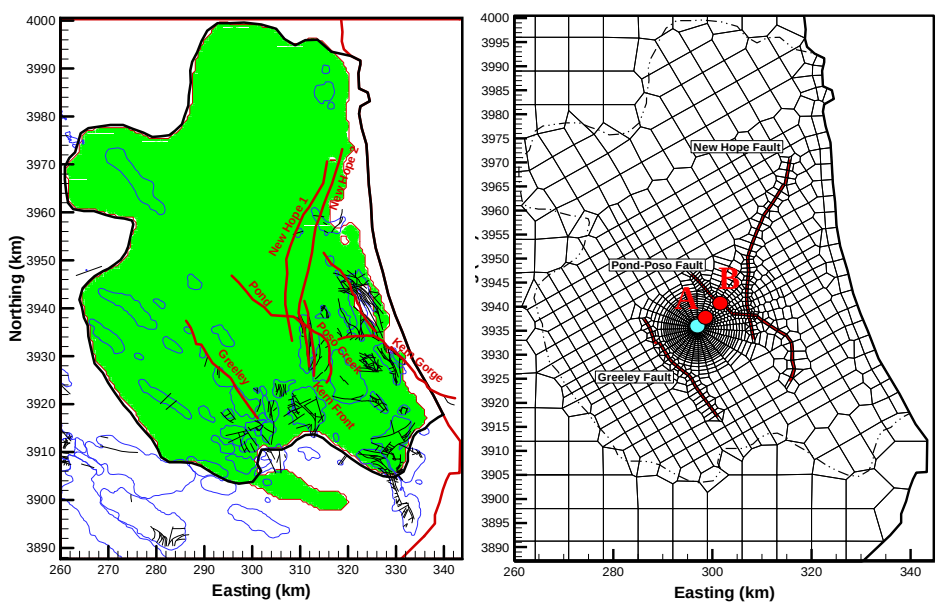

(a) (b)

Figure 1: (a) Plan view of the Vedder formation and the faults (the major faults are shown in red.), and (b) Plan view of the numerical domain with mesh. The blue dot is the injection location, and the red dots (Point A and B) are used as points of interest in this study.

Figure 1(a) also shows the outline of several faults in the area. Fault zone properties are quite uncertain; however, there are qualitative observations that most fault zones should be less conductive than the adjacent sandstone formations (Birkholzer et al., 2011): (1) oil and gas trapping is observed under in situ effective stress conditions, (2) water-level observations in the Pond-Poso-Creek fault zone east of the hypothetical injection location suggest a partial groundwater barrier in shallow units, and (3) oil and gas fields are partially compartmentalized as evidenced by pumping tests. While acting as partial barriers, the fault offset is in all cases significantly smaller than the thickness of the Vedder formation; thus some lateral hydraulic connectivity across the faults is to be expected. For the purpose of this study, partial compartmentalization was assumed as a fault scenario such that the lateral fault permeability of major faults is reduced by a factor of 100 compared to the adjacent formation permeability. The model explicitly accounts for the three most prominent faults in the numerical grid (Figure 1b): the Greeley fault west of the injection location, as well as the Pond-Poso-Creek fault zone and the New Hope fault zone east of the injection location. Additional fault property scenarios were studied, but shall not be reported here. Note that in all scenarios, faults are assumed non-conductive in shale formations; i.e., the potential for leakage of CO_2 and/or brine through permeable faults is not a concern in this study. Also, the potential for fault reactivation is not addressed in this study.

The massively parallel version of TOUGH2 (Zhang et al., 2008) was used with the ECO2N module to simulate injection and migration of supercritical CO_2 in the brine system. The ECO2N module describes thermodynamics and thermophysical properties of H_2O-NaCl-CO_2 mixtures, including phase transitions and dissolutions (Pruess, 2005). The simulation time includes the injection period of 50 years with an injection rate of 5 Mt per year, and a post-injection period of 150 years. In this study, a 3D mesh of 64,214 elements was generated for 16 hydrogeological layers, representing the 11 formations from the crystalline base rock to the top shallow aquifer. As mentioned before, the storage formation (the Vedder sandstone) was divided into three sand model layers and three alternating shale layers (V Sand and V Shale). This mesh was obtained by coarsening the high-resolution mesh used by Zhou et al. (2011) and Zhou and Birkholzer (2011); it was more refined both laterally and vertically than the coarse mesh used in Birkholzer et al. (2011). The mesh design was such that this study can accommodate a large number of simulations, while accurately accounting for the CO_2 plume behavior in the storage formation. Figure 1b shows the plan view of the current numerical mesh. Significant mesh refinement can be seen in the center of the domain, where multi-phase processes and strong pressure buildup can be expected in response to CO_2 injection.

For discussion of sensitivity analysis, one needs to choose performance measures, which depends on the type of model application and the focus of a given study. These performance measures may be point-based, such as localized CO_2 saturation and localized pressure, or they may be area-based, such as CO_2 plume extent and spatial extent of pressure buildup above a given threshold (Nicot et al., 2008). In this study, three measures were chosen, two of which are point-based: CO_2 saturation at a point 1.8 km updip from the injection location (Point A in Figure 1b), and pressure buildup at the fault 7.3 km updip from the injection point (Point B in Figure 1b). The third measure is the extent of the overpressure zone, which is defined here as the area of pressure increase larger than 0.2 MPa at the reservoir-caprock interface.

3. SENSITIVITY ANALYSIS METHODS AND IMPLEMENTATION

This section introduces the three sensitivity methods. Although each method is documented in detail in Morris (1991) and Saltelli et al. (2008), they are briefly described here for completeness. A set of parameters are denoted by $\{x_i | i=1,\ldots,k\}$ and a scalar output of a model by y, which is a function of $\{x_i\}$; $y = f(\{x_i\})$, where k is the number of parameters.

3.1 LOCAL SENSITIVITY METHOD

The local sensitivity is defined as a partial derivative, i.e., the change of an output variable caused by a unit change in each parameter from the reference value. A numerical model can compute the derivative by changing each parameter by a small increment Δx_i from the reference parameter values x_i^* and computing the difference of the output. The scaled sensitivity is the derivative scaled by the standard deviation of parameters and measurement errors. The scaled, dimensionless sensitivity is defined as:

$$S_i^{local} = \frac{\sigma_x}{\sigma_y} \frac{\partial y}{\partial x_i}\bigg|_{x_i*} = \frac{\sigma_x}{\sigma_y} \frac{f(x_1*,..,x_i*+\Delta x_i,..) - f(x_1*,..,x_i*,..)}{\Delta x_i} \quad . \tag{1}$$

where σ_x is the standard deviation of the parameter, and σ_y is the standard deviation of the model output, reflecting its measurement error or acceptable mean residual in an inversion.

3.2 MORRIS SENSITIVITY METHOD

In the Morris one-at-a-time (OAT) method (Morris, 1991), the parameter range—normalized as a uniform distribution in [0, 1]—is partitioned into (p–1) equally-sized interval so that each parameter takes values from the set $\{0, 1/(p-1), 2/(p-1), \ldots, 1\}$. From the reference point of each parameter randomly chosen from the set $\{0, 1/(p-1), 2/(p-1), \ldots, 1-\Delta\}$, the fixed increment $\Delta = p/\{2(p-1)\}$ is added to each parameter in a random order to compute an elementary effect (EE) of each parameter, which is the difference of output y caused by the change in the respective parameter. k+1 runs are necessary to complete one path, which is to change each parameter once from one set of reference values. By having multiple paths (i.e., multiple sets of reference parameter values and multiple, random orders of changing each parameter), there is an ensemble of EEs for each parameter. Three statistics can be computed: the mean of EE, variance of EEs, and the mean of absolute EEs (mean of |EE|). The mean EE can be regarded as a global sensitivity measure. The mean |EE| is used to identify non-influential factors. The variance of EE is used to compute the standard error of mean (SEM) for identifying nonlinear or interaction effects.

3.3 SALTELLI SENSITIVITY METHOD

While the local and Morris sensitivity methods are difference-based, the Saltelli method is variance-based. Saltelli et al. (2008) defined the sensitivity index by $\mathbf{V}[\mathbf{E}[Y|X_i]]/\mathbf{V}[Y]$ for parameter importance, where $\mathbf{E}[\bullet]$ and $\mathbf{V}[\bullet]$ represent mean and variance, respectively. This is the variance of conditional expectation of the system response when Parameter i is fixed, normalized by the total variance of system response. Conceptually, this measure quantifies the contribution of each parameter to the uncertainty or variability of the output. In addition, Saltelli et al. (2008) defined the total sensitivity index by $\mathbf{V}[\mathbf{E}[Y|X_{-i}]]/\mathbf{V}[Y]$, where $\mathbf{E}[Y|X_{-i}]$ represents the

mean of Y conditioned on all the parameters but X_i. The total sensitivity is used to identify unimportant parameters. These two indices can be computed using the Monte-Carlo integration described in Saltelli (2002, 2008).

3.4 IMPLEMENTATION IN iTOUGH2

The global sensitivity analysis module was implemented in iTOUGH2 (Finsterle, 2010). iTOUGH2 was coupled with TOUGH2-MP using the PEST protocol (Doughty, 2007; Finsterle and Zhang, 2011). Typically, the sensitivity analysis is done in serial by generating sets of parameters, running the simulations and analyzing the simulation results. This scheme is often problematic for large-scale simulations when there are numerical problems caused by a few set of parameters and the entire run is too expensive to repeat. To accommodate large-scale reservoir simulations, iTOUGH2 was modified so that it can decouple the scheme into three parts.

> *Part 1: Pre-processing.* In a pre-processing step, iTOUGH2 generates input parameters and writes input files from the parameter distributions, and saves them in directories.
>
> *Part 2: Simulations*. iTOUGH2 or a simple script initiates embarrassingly parallel runs of TOUGH2-MP.
>
> *Part 3: Post-processing.* In a post-processing step, iTOUGH2 reads the output files from each directory and analyzes them, for example, by calculating sensitivity coefficients, composite sensitivity measures, or elementary effects and their variances.

Since all the related files are stored in each directory, when a few parameter sets cause numerical problems, it is possible to investigate the cause and fix each one of them without repeating the entire analysis. The post-processing procedure can later include the fixed results.

This three-step approach also provides more flexibility; it is possible to re-analyze the output for different performance measures. The pre-processing part is data or physics driven such that once the data and model is established the parameter distributions and the input files can be fixed. The post-processing part is application driven so that many performance measures can be considered for different applications (e.g., leakage, induced seismicity). Since all the output files are kept, iTOUGH2 can analyze different measures without re-running the simulations, which are the most expensive part.

4. PARAMETER DISTRIBUTION

In this SA, five properties (permeability, porosity, pore compressibility, van Genuchten α and m) are varied of two geological layers of the storage formation (V Sand and V Shale) and the caprock (TF Shale), so that there is a total of 15 parameters. For the V Sand permeability and porosity, the depth-dependent parameter values and their uncertainty range were estimated using available datasets (Figure 2). For the rest of the parameters, the reference parameter values are shown in Table 1. The range of parameters in this study is one order of magnitude up and down in permeability, a factor of five up and down in pore compressibility, 30% up and down in porosity and van Genuchten m, and half an order of magnitude up and down in van Genuchten α. For brevity, the hydrogeologic properties of all other model layers, which are kept constant in the SA, are not provided in this report (see Birkholzer et al., 2011, for further information).

Table 1: Reference parameter values: horizontal permeability k_h, anisotropy ratio k_v/k_h, porosity Φ, pore compressibility β_p, van Genuchten α and m.

	TF Shale	V Sand	V Shale
k_h, mD	0.002	*dep-dep.	0.1
k_v/k_h	0.5	0.2	0.5
Φ	0.338	*dep-dep.	0.32
β_p, 10^{-10} Pa^{-1}	14.5	4.9	14.5
α, 10^{-5} Pa^{-1}	0.42	13	0.42
m	0.457	0.457	0.457

* Depth-dependent values shown in Figure 2.

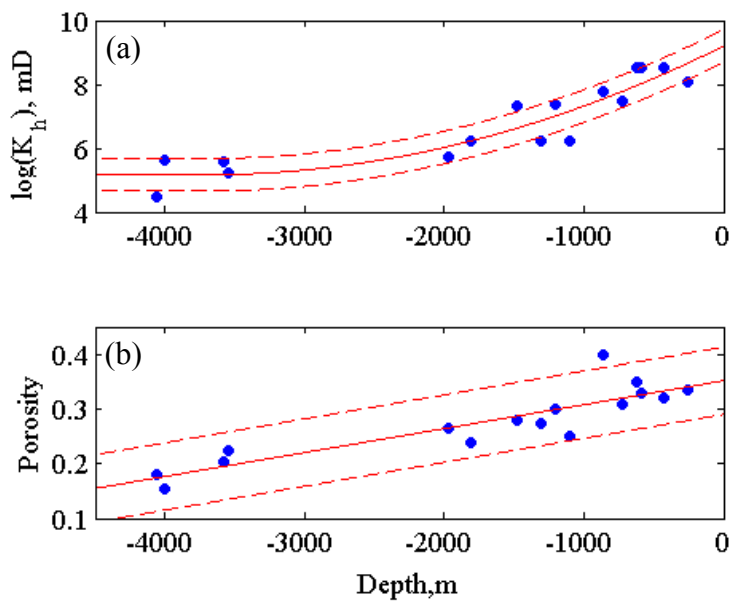

Figure 2: Estimated depth-dependent (a) V Sand permeability (natural logarithm), and (b) V Sand porosity. The blue dots are the data values, the solid red line is the estimated value, and the dotted red lines are ± two standard deviations.

For the V Sand permeability and porosity, data exists from sixteen hydrocarbon fields in the domain. Since a clear depth dependency was observed, as is shown in Figure 2, the trend associated with the depth was removed. A quadratic function was fitted for log-permeability, using a flat value below the vertex point. For porosity, a linear trend was assumed, since changing it to a quadratic function did not significantly decrease the residual (less than 1%). After the trend removal, Gaussian distributions for log-permeability and porosity were assumed. The standard deviation (STD) is 5.1E-1 and 3.1E-2 for log-permeability and porosity, respectively. Equations (2) and (3) define the trend parameters for the V Sand log-permeability ($\log k_h$) and porosity (Φ) as a function of elevation (z) and mean elevation ($\mu_z = -1723$m), shown in Table 1.

$$\log k_h = p_2 (z - \mu_z)^2 + p_1 (z - \mu_z) + p_0, \qquad \text{if } z > -3710 \text{ m} \tag{2}$$

$$p_0, \qquad \text{otherwise}$$

$$\Phi = p_1(z - \mu_z) + p_0 \tag{3}$$

Table 2: Trend parameters for V Sand log-permeability and porosity

	p_0	p_1	p_2	STD
$\log k_h$	6.32	1.16e–3	2.93e–7	0.511
Φ	0.276	4.37e–5		3.08e–2

5. RESULTS

5.1 BASE-CASE SIMULATION

Figure 3 shows the plume evolution and pressure buildup at the reservoir-caprock interface. The pressure response to CO_2 injection is fast and eventually affects a large region close to all the boundaries. The semi-permeable faults clearly affect the pressure response by confining the pressure buildup to the region of injection inside the faults. At the end of injection, the highest pressure occurs towards the updip direction of the fault. After injection, the pressure dissipates and returns back close to the hydrostatic.

On the other hand, the CO_2 plume migrates slowly. At the end of injection, the CO_2 plume stays within a 5.0 km radius from the injection point. After injection ends, the plume continues migrating eastward driven by buoyancy, until it arrives at the fault around 100 years and is stopped from further migration.

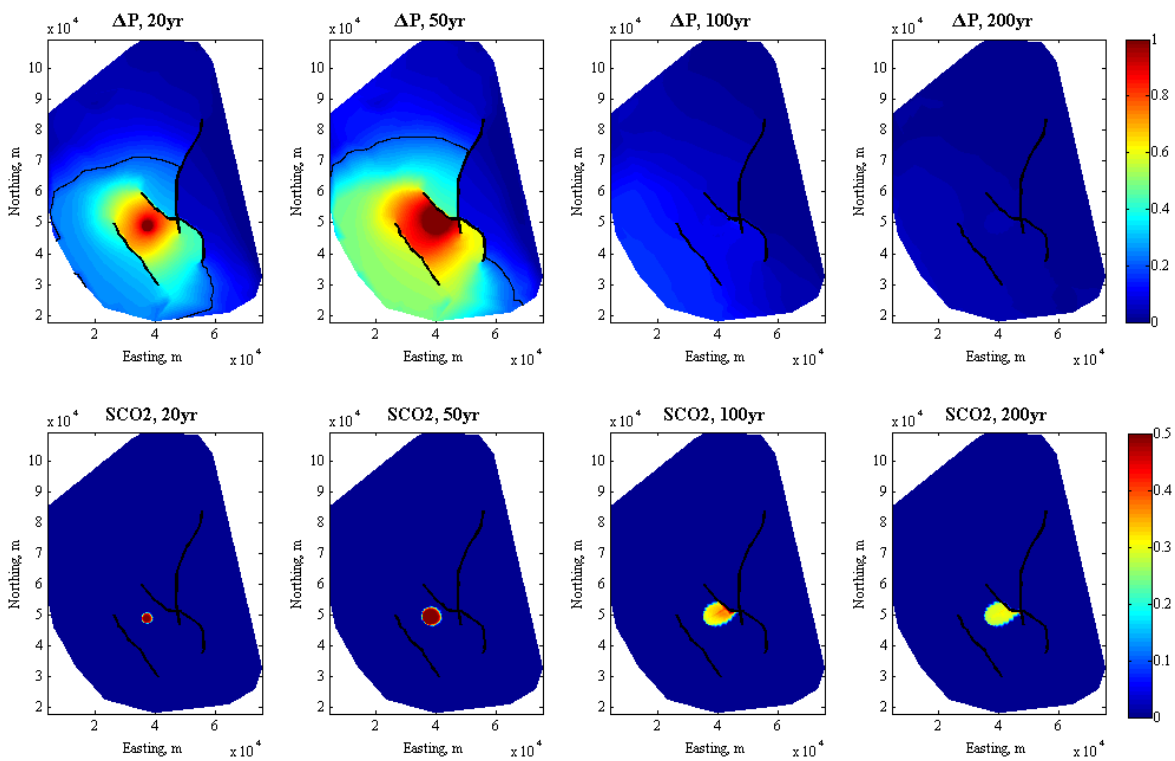

Figure 3: Evolution of pressure buildup (top row; ΔP in MPa) and CO_2 saturation (bottom row) at 20, 50, 100 and 200 yr (left to right columns). The solid thick black lines are fault locations. The thin black lines in the pressure buildup plots represent the 0.2 MPa-contour line.

Figure 4 shows the time profiles of the three selected performance measures: CO_2 saturation at Point A, pressure buildup at Point B, and spatial extent of overpressure zone (the area of pressure increase larger than 0.2 MPa at the reservoir-caprock interface). In Figure 4a, the CO_2 saturation quickly increases as the plume arrives. After plume departure, the saturation decreases towards the residual saturation of 0.3. In Figure 4b, the pressure buildup occurs more smoothly. After the

peak at the end of the injection period (50 years), the pressure buildup decays towards zero. In Figure 4c, the overpressure zone increases quickly up to around 20 years, after which the increase slows down considerably. The distinct gradient changes (or bumps) can be seen in the overpressure-zone curve, which can be attributed to the pressure field reaching the lateral faults or arriving at the formation boundaries. In the post-injection period, the overpressure zone decreases quickly, again showing a steps-wise behavior; the transition of the steps (around 60 years and 75 years) corresponds to the time when the pressure extent passes through the faults.

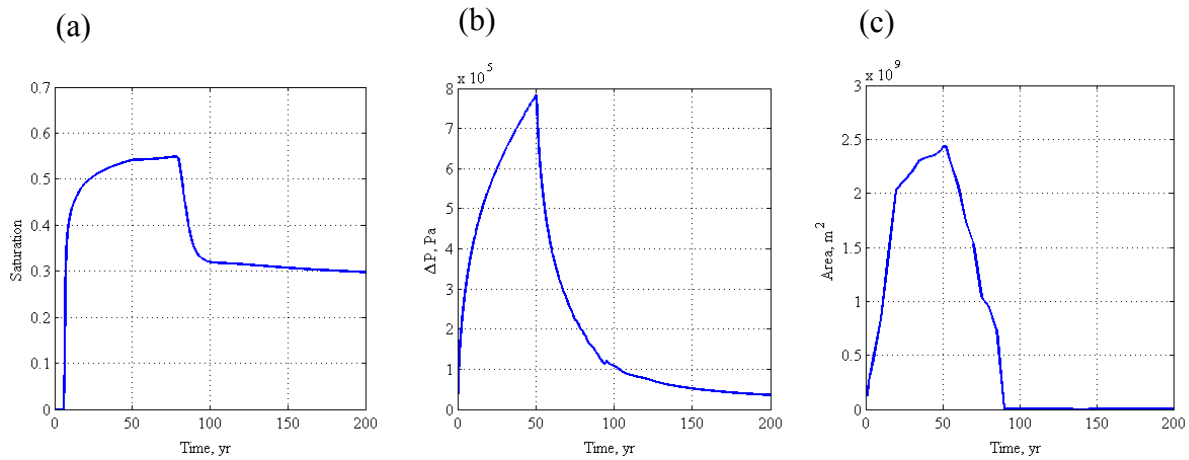

Figure 4: Time profile of the performance measures for the reference parameter case: (a) CO_2 saturation (S_{CO2}), (b) pressure buildup (ΔP), and (c) overpressure zone.

5.2 UNCERTAINTY ANALYSIS

To illustrate the overall effect of the parameter variations discussed in Section 4, 200 sets of parameters were generated for a Monte Carlo study, using the Latin hypercube scheme to sample from the Gaussian distributions with the variance being half of the parameter range. Figure 5 shows 200 realizations of the three performance measures as a function of time; it illustrates the considerable variability in results stemming from the uncertainty in model inputs.

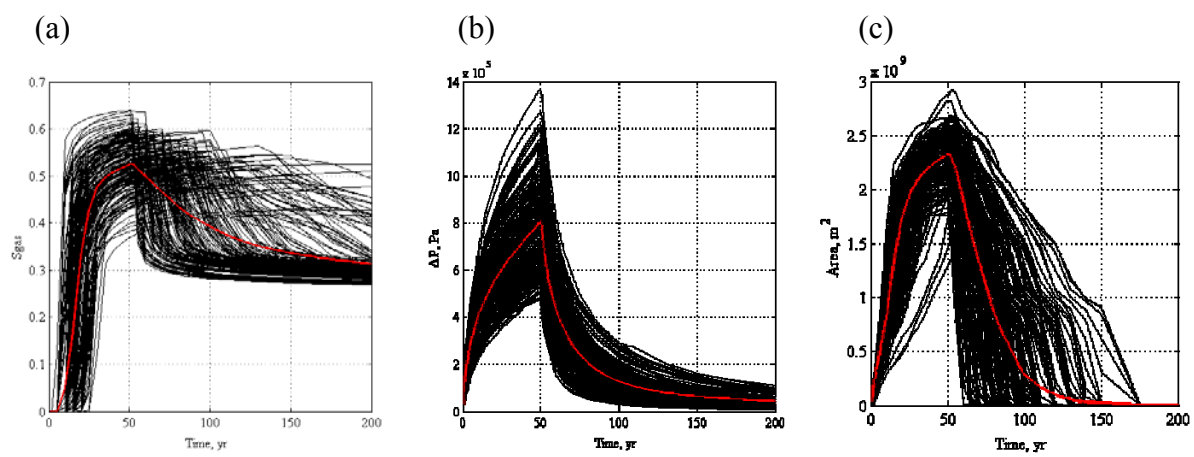

Figure 5: Monte-Carlo simulation results; time profiles of the performance measures: (a) CO_2 saturation (S_{CO2}), (b) pressure buildup (ΔP), and (c) overpressure zone. The red line is the mean at each time slice.

5.3 LOCAL SENSITIVITY

The local sensitivity was computed using sixteen simulations. Figure 6 shows the time series of local sensitivity for three performance measures. In Figure 6a, for CO_2 saturation (S_{CO2}) at Point A, there are three dominant parameters: permeability (k), porosity (Φ), and van Genuchten m, for the reservoir (V Sand). All three curves have two spikes, which correspond to the plume arrival and departure. Higher permeability and m lead to higher plume/brine mobility, which leads to positive sensitivity at the plume arrival (i.e., earlier arrival and higher S_{CO2}) and negative sensitivity at plume departure (i.e., earlier departure and lower S_{CO2}). The large porosity means more CO_2 can be stored per unit volume of porous media by displacing resident brine at the arrival and more CO_2 at the departure, so that porosity has the opposite effect of permeability and m. This result may support the development of simple analytical or semi-analytical solutions, or decoupled reservoir-only CO_2 migration models. For example, this study found that the van Genuchten α has a negligible effect on far-field CO_2 saturation, consistent with some of the analytical studies that neglect the capillary pressure (e.g., Nordbotten et al., 2009).

The pore-size distribution index m has a large impact at the arrival but less at the departure. This is attributed to the specific implementation of the two-phase model in the current version of TOUGH2-MP/ECO2N, which uses the van Genuchten model for relative brine permeability (k_{lr}) and capillary pressure, and the Corey model for relative gas permeability—so that the relative gas permeability does not depend on m (Pruess et al., 1999). Since the derivative of relative brine permeability with respect to m ($\partial k_{lr}/\partial m$) increases in absolute magnitude towards full brine saturation, m is more influential near full brine saturation and hence at plume arrival. This result may change once the van Genuchten model with the hysteresis (Doughty, 2007) is implemented in TOUGH2-MP, which makes CO_2 relative permeability dependent on m. The point to address here is that the sensitivity analysis is useful in identifying and understanding an effect that is potentially an artifact of model implementation.

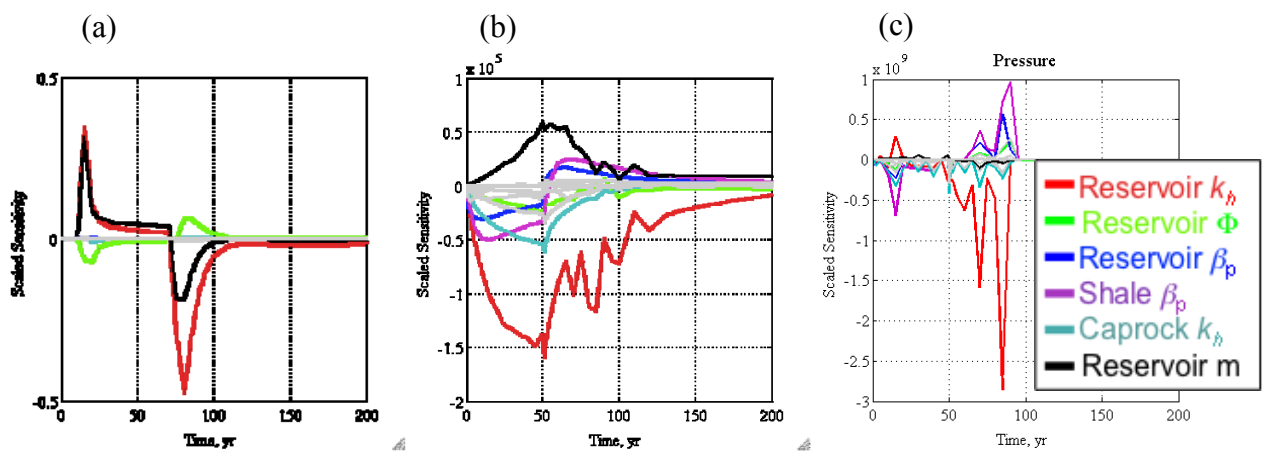

Figure 6: Local sensitivity results. (a) CO_2 saturation at Point A, (b) pressure buildup at Point B, and (c) overpressure zone. Six most significant parameters are colored and labeled.

For the pressure buildup at Point B (Figure 6b), in addition to permeability and m, the sensitivity to V Sand (reservoir) and V Shale compressibility (β) and TF Shale (caprock) permeability is visible. Although the profile is smoother than that of CO_2 saturation, there is some oscillation around 85 years, which corresponds to the time of plume arrival at this location. The V Sand and

TF Shale permeabilities have similar sensitivity trends, although the magnitude is different. This is because both are related to the dissipation of pressure in the system. The V Sand and V Shale compressibilities have a negative effect during injection, and a positive effect in the post-injection period; higher compressibility creates larger absorption of pressure in the pore framework during the injection, and slower recovery (hence higher pressure) in the post-injection period.

It is interesting to note that V Sand *m* has a positive sensitivity index on pressure, while reservoir permeability has a negative sensitivity index. This behavior is different from the CO_2 saturation at Point A, where V Sand *m* and reservoir permeability follow the same sensitivity trend. A higher reservoir permeability reduces pressure over the entire domain, explaining the negative sensitivity. Changing the V Sand *m* parameter affects only the brine-CO_2 mixture within the plume. Since a higher *m* increases the brine relative permeability in the brine-CO_2 mixture, it accelerates plume migration and therefore increases the pressure outside the plume (thus a positive sensitivity).

The overpressure zone in Figure 6c shows several spikes. These spikes correspond to the times when the boundaries of the overpressure zone arrive at pass through the faults. Reservoir permeability has first a positive spike since the larger permeability gives rise to a larger extent of the overpressure zone. In the post-injection period, the higher permeability helps the pressure to dissipate faster. The reservoir and shale compressibility have opposite effects.

5.4 MORRIS SENSITIVITY

In the Morris method, the EEs were computed using four partitions and ten paths. The total number of simulations was 160. Figure 7 shows the time profiles of mean EE from the Morris method. Although the mean of absolute EEs is computed as well, the results are not shown here, since the mean of absolute EEs did not provide additional information in this case. This is because the sign of EEs was mostly the same at each time slice so that the mean of absolute EEs was equal to the mean of EEs.

Compared to the local sensitivity in Figure 6, the spikes are smoothed out over time, since the plume arrival/departure or pressure breakthrough time is more distributed. In terms of importance ranking and sign of effects, a conclusion is drawn similar to the local sensitivity analysis such as the V Sand permeability being a dominant parameter. However, there are some differences compared to the local sensitivity.

In Figure 7a for the CO_2 saturation at Point A, although the same three parameters are being identified as most influential, the porosity effect is more prominent at early times, and the V Sand permeability becomes dominant in the post-injection period. In Figure 7b for the pressure buildup at Point B, the sensitivity to the V Sand compressibility increases but sensitivity to the V Shale compressibility is smaller. In Figure 7c for the overpressure zone, sensitivity to reservoir compressibility and TF Shale permeability appear at early times.

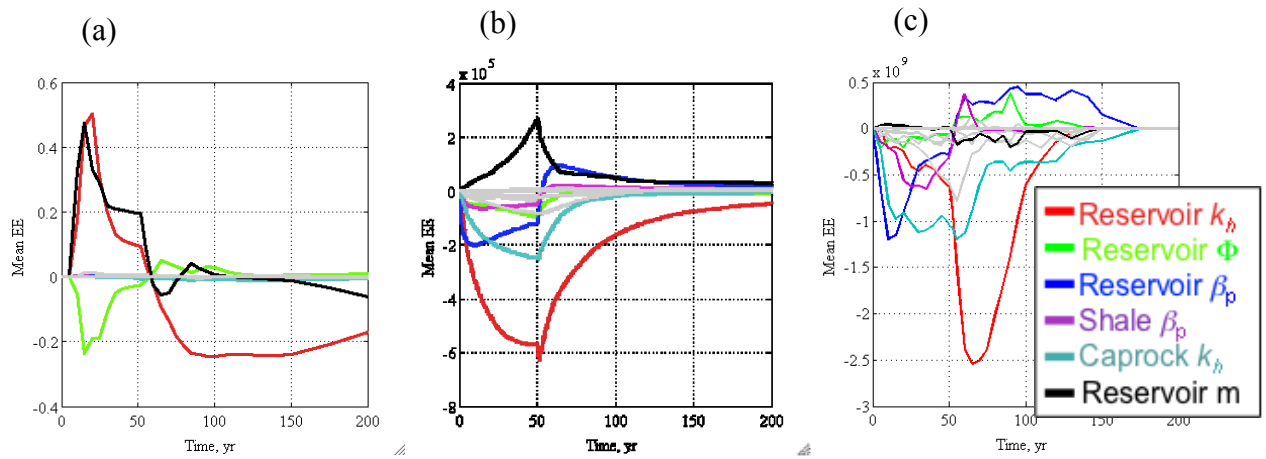

Figure 7: Morris sensitivity results. (a) CO_2 saturation at Point A, (b) pressure buildup at Point B, and (c) overpressure zone. Six most significant parameters are colored and labeled.

In addition, a cross-plot of mean EE and standard deviation of EE (STD) at one time slice (20 years) is shown in Figure 8. In this figure, parameters with higher STD, i.e., those that are closer to the black solid lines (Mean EE = ±2SEM), exhibit stronger nonlinearity or interaction effects. Note that the standard error of mean (SEM) was computed using the variance of EE and the number of paths. The parameters below the lines have a significant effect on the response, since 2SEM represents the confidence interval of estimating the mean EE.

In Figure 8a for the point CO_2 saturation, the reservoir permeability and *m* have large mean EE and low SEM values; the porosity is close to the black line, indicating nonlinearity or interaction effects. In Figure 8b for the point pressure buildup, the reservoir and shale compressibility is close to the line. In Figure 8c for the overpressure zone, all the parameters are relatively close to the line compared to Figure 8a and b. In general, it was observed that parameters with higher SEM generally exhibit significant differences between results from the local sensitivity and Morris sensitivity analyses.

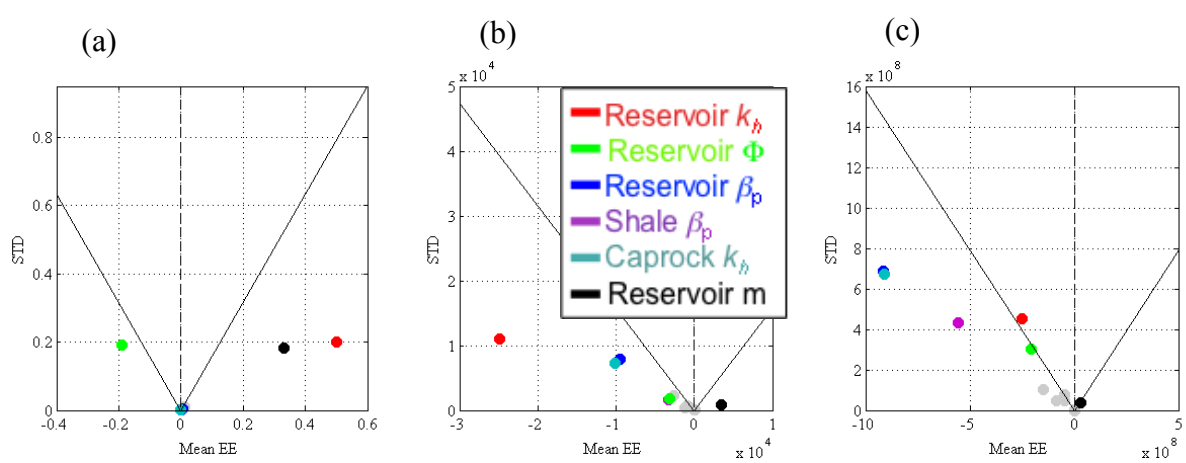

Figure 8: Morris sensitivity results. Mean EE vs. STD: (a) CO_2 saturation at Point A, (b) pressure buildup at Point B, and (c) overpressure zone. Six most significant parameters are colored and labeled.

5.5 SALTELLI SENSITIVITY

Based on the results from the Morris method shown in Figure 7, five parameters were chosen for the Saltelli sensitivity analysis (V Sand permeability, porosity, compressibility, *m*, and TF Shale permeability). Saltelli sensitivities using 840 realizations were computed. Sets of parameters by Latin hypercube sampling were generated assuming the Gaussian distribution with the standard deviation being half of the range specified in Section 4. Figure 9 shows the time profile of Saltelli sensitivity. The sensitivity is normalized by the variance at each time slice, so that there are no peaks such as those that appeared in the Morris sensitivity in Figure 7. The sum of the sensitivity of each parameter, however, does not become one, since there exist nonlinear or interaction effects (Saltelli, 2008).

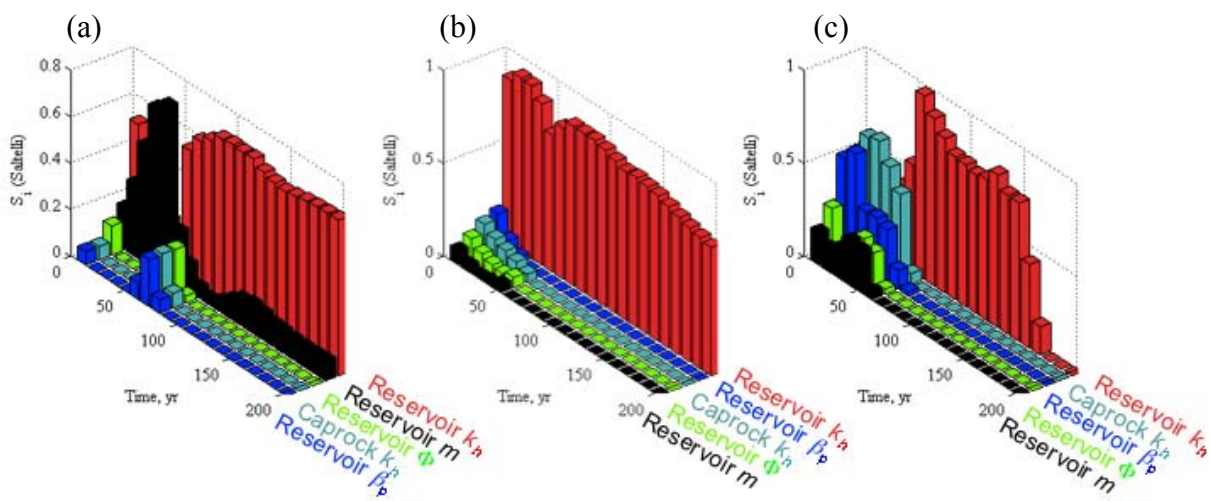

Figure 9: Saltelli sensitivity results (a) CO_2 saturation at Point A, (b) Pressure buildup at Point B, and (c) Overpressure extent.

From this figure, more quantitative measures of sensitivity could be defined. For example, in Figure 9a for CO_2 saturation in Point A, the V Sand van Genuchten *m* accounts for about 70% of the total variability of the output at time 30–50 years, while the V Sand permeability accounts for about 70% after 100 years (most of the post-injection period). The qualitative interpretation and ranking, however, are similar to the Morris mean EE, although the magnitude is different in some cases.

6. DISCUSSION AND CONCLUSION

6.1 COMPARISON OF THREE SENSITIVITY METHODS

The results show that all the three considered sensitivity methods give similar interpretations and importance rankings, except when a parameter has a strong nonlinear effect or interacts with some other parameters—which is the case when a global SA is warranted. The local sensitivity appears sufficient to identify the most influential parameters in this study. Even for cases with nonlinear or interaction effects, the local sensitivity is still useful in improving system understanding (e.g., the high sensitivity of plume arrival/departure to parameters affecting CO_2 mobility). The sign of sensitivity (i.e., positive and negative effects) is useful to interpret and understand the effect of each parameter (e.g., permeability for dissipating the pressure) and to confirm the results by comparing them to intuition. The interpretation of the local sensitivity results helps understand the results from the Morris or Saltelli methods as well.

The Morris sensitivity method has many uses, such as identifying positive or negative effects, and also selecting influential parameters. The mean EE, which is computed from many different reference values over the parameter space, can be considered as an averaged version of local sensitivity. The standard deviation of EE can be used to identify the presence of nonlinear or interaction effects. Plotting the mean EE and STD is useful to compare the parameter importance in the presence of nonlinearity/interactions. The advantage of the Morris method is the significance of sensitivity measures (e.g., Mean EE) under nonlinearity or interactions. The computational burden was relatively small compared to the Saltelli method.

The Saltelli sensitivity method yields more rigorous and quantitative sensitivity measures in the context of UQ such as how much each parameter is responsible for the variability of the response. This measure would be useful to determine which parameter to neglect, considering X% of the variability in the system response during the risk assessment. One disadvantage is that as a variance-based measure, the Saltelli method does not provide the sign of the sensitivity (i.e., negative/positive effect), which is useful for the system understanding. The computational requirement is high, since it is based on Monte Carlo integration.

6.2 IMPLICATIONS FOR THE CO_2 STORAGE SYSTEM

This study found that only three parameters are relevant on the predicted CO_2 saturation: the reservoir (V Sand) permeability, porosity, and van Genuchten *m*. This would justify developing a simplified model, such as assuming a no-flow boundary at the reservoir-caprock interface without including the caprock, or neglecting the capillary pressure (e.g., Saripalli and McGrail, 2002; Nordbotten et al. 2005; Nordbotten et al., 2009). The relative permeability, however, needs to be accounted accurately, since the sensitivity to van Genuchten *m* implies the importance of relative permeability of brine and CO_2. To improve this model, it is essential to investigate the impact of different two-phase models, and also to account for hysteresis.

It is surprising that the inter-bedded shale layers (V Shale) do not have any impact on the CO_2 saturation. It is not because heterogeneity is not important, but rather because the V Shale is continuous and always has much lower permeability than the V Sand in this analysis. As a result the CO_2 plume does not enter the V Shale, but migrates horizontally through the sand layers. If the V Shale permeability became closer to that of V Sand or the V Shale layers were discontinuous, the CO_2 could migrate through the shale layers vertically due to buoyancy, which

would change the CO_2 saturation. Indeed the presence of the V shale layers affects the CO_2 plume extent and the arrival time to a point of interest in Zhou and Birkholzer (2011). It also implies that the interpretation of sensitivity is limited to the conceptual model (i.e., having continuous low-permeability shale layers in the reservoir).

The pressure response depends on more parameters than the CO_2 saturation, i.e., it is also sensitive to changes in the V Sand and V Shale compressibilities and TF shale (caprock) permeability. This confirms the findings from previous studies (e.g., Birkhozer, 2011), concluding that pressure-related risk analyses, such as induced seismicity, require a large-scale reservoir model that includes multiple layers.

The time frames for pressure propagation and CO_2 plume migration are different and so are the related sensitivities. The pressure buildup becomes highest at the end of the injection period, and quickly decays afterwards, whereas the CO_2 plume keeps migrating beyond the injection period and stays above the residual saturation, although the CO_2 plume extent is fairly limited during the injection. This implies that although the pressure-related risks disappear quickly after the injection ends, the CO_2 leakage risk might persist for a longer time and in a larger area, since the CO_2 can leak by buoyancy forces without overpressure. This feature will affect the risk profiles as a function of time. In particular, the risks of brine leakage may peak earlier than the risks of CO_2 leakage, as the former mostly depends on the pressure buildup, while the latter depends on the CO_2 extent and the locations of leaky pathways.

The sensitivity results showed a clear trend of long-term sensitivity dominated by a few parameters, especially the permeability of the injection reservoir. While looking at a limited sample here (i.e., saturation at Point A, pressure buildup at Point B, and overpressure extent), one may infer from such results that long-term risk can be better predicted if reservoir permeability is well constrained. Fortunately, since the reservoir permeability also has a large impact on the pressure buildup during the injection, the permeability uncertainty could be reduced by history-matching during CO_2 injection using an appropriate monitoring strategy. In addition, the findings in this study point to the importance of basic research focused on better understanding and characterizing intrinsic and/or relative permeability in the reservoir, including effects of spatial and temporal heterogeneity (e.g., Li et al., 2011).

Readers, however, should be aware that this study is limited to the parameter sensitivities affecting CO_2 saturation and pressure in the reservoir, although many insights were gained for the potential risks related to CO_2 storage. Because the reservoir model in this study is not connected to actual leakage pathways, this study cannot answer the question as to how uncertainties in the reservoir may propagate into uncertainties of leakage rates and actual risk measures. An integrated sensitivity analysis—including the reservoir model, risk pathway models, and possibly risk effect models—would be needed to address which parameter in the reservoir model is the most important for a particular type of risk.

7. REFERENCES

Birkholzer, J.T.; Zhou, Q.; Cortis, A.; Finsterle, S. A sensitivity study on regional pressure buildup from large-scale CO_2 storage projects. *Energy Procedia* **2011,** *4*, 4371-4378.

Cacuci, D.G. *Sensitivity and uncertainty analysis*, Vol. 1: Theory; Chapman and Hall/CRC Press: Boca Raton, FL, 2003.

Doughty C. Modeling geologic storage of carbon dioxide: comparison of non-hysteretic and hysteretic characteristic curves. *Energy Conversion and Management* **2007,** *48*(6), 1768-1781.

Finsterle, S. *iTOUGH2 User's Guide*; Report LBNL-40040; Lawrence Berkeley National Laboratory: Berkeley, CA, 2010.

Finsterle, S.; Zhang, Y. Solving iTOUGH2 simulation and optimization problems using the PEST protocol. *Environmental Modeling and Software* **2011,** *26*, 959–968.

Finsterle, S., M.B. Kowalsky and K. Pruess, TOUGH: Model use, calibration and validation. *Transactions of the ASABE* **2012,** *55*(4), 1275–1290.

Li, S.; Zhang, Y.; Zhang, X. A study of conceptual model uncertainty in large-scale CO_2 storage simulation. *Water Resour. Res.* **2011,** *47*, W05534.

Morris, M.D. Factorial sampling plans for preliminary computational experiments. *Technometrics* **1991,** *33*(2), 161-174.

Nicot, J.-P.; Oldenburg, C.M.; Bryant, S.L.; Hovorka, S.D. Pressure perturbations from geologic carbon sequestration: Area-of-review boundaries and borehole leakage driving forces. Presented at the 9th International Conference on Greenhouse Gas Control Technologies (GHGT-9), Washington, D.C., November 16-20, 2008; GCCC Digital Publication Series #08-03h.

Nordbotten, J. M.; Celia, M. A.; Bachu, S. Injection and storage of CO_2 in deep saline aquifers: analytical solution for CO_2 plume evolution during injection. *Transport in Porous Media* **2005,** *58*(3), 339-360.

Nordbotten, J. M.; Kavetski, D.; Celia, M. A.; Bachu, S. Model for CO_2 leakage including multiple geological layers and multiple leaky wells. *Environ. Sci. and Technol.* **2009,** *43* (3), 743-749.

Pau, G.; Zhang, Y.; Finsterle, S. Reduced order models for subsurface flow in iTOUGH2. Proceedings from the TOUGH Symposium 2012, Lawrence Berkeley National Laboratory, Berkeley, California, September 17-19, 2012.

Pruess, K.; Oldenburg, C.; Moridis, G. *TOUGH2 User's Guide, Version 2.0*; Report LBNL-43134; Lawrence Berkeley National Laboratory, Berkeley, CA, 1999.

Pruess, K. *ECO2N: A TOUGH2 fluid property module for mixtures of water, NaCl, and CO_2*; Report LBNL-57952; Lawrence Berkeley National Laboratory, Berkeley, CA, 2005.

Saltelli, A. Making best use of model evaluations to compute sensitivity indices. *Computer Physics Communications* **2002,** *145*, 280-297.

Saltelli, A.; Ratto, M.; Tarantola, S.; Campolongo, F.; European Commission Joint Research Centre of Ispra (I). Sensitivity analysis practices: Strategies for model-based inference. *Reliability Engineering and System Safety* **2006,** *91* (10-11), 1109-1125.

Saltelli, A.; Ratto, M.; Andres, T.; Campolongo, F.; Cariboni, J.; Gatelli, D.; Saisana, M.; Tarantola, S. *Global sensitivity analysis: The Primer*, John Wiley and Sons, 2008.

Saripalli P.; McGrail, B.P. Semi-analytical approaches to modeling deep well injection of CO_2 for geological sequestration. *Energy Conversion and Management* **2002,** *43*(2), 185-198.

Zhang, K.; Wu, Y.S.; Pruess, K. *User's Guide for TOUGH2-MP – A massively parallel version of the TOUGH2 code*; Report LBNL-315E; Lawrence Berkeley National Laboratory, Berkeley, CA, 2008.

Zhou, Q.; Birkholzer, J.T.; Wagoner, J.L. Modeling the potential impact of geologic carbon sequestration in the southern San Joaquin basin, California. *Presented at The Ninth Annual Carbon Capture & Sequestration*; Pittsburgh, PA, May 2011.

Zhou, Q.; Birkholzer, J.T. On scale and magnitude of pressure build-up induced by large-scale geologic storage of CO_2. *Greenhouse Gases: Science and Technology* **2011,** *1*, 11-20.

nrap
National Risk
Assessment Partnership

NRAP is an initiative within DOE's Office of Fossil Energy and is led by the National Energy Technology Laboratory (NETL). It is a multi-national-lab effort that leverages broad technical capabilities across the DOE complex to develop an integrated science base that can be applied to risk assessment for long-term storage of carbon dioxide (CO_2). NRAP involves five DOE national laboratories: NETL-RUA, Lawrence Berkeley National Laboratory (LBNL), Lawrence Livermore National Laboratory (LLNL), Los Alamos National Laboratory (LANL), and Pacific Northwest National Laboratory (PNNL). The NETL-RUA is an applied research collaboration that combines NETL's energy research expertise in the Office of Research and Development (ORD) with the broad capabilities of five nationally recognized, regional universities—Carnegie Mellon University (CMU), The Pennsylvania State University (PSU), the University of Pittsburgh (Pitt), Virginia Tech (VT), and West Virginia University (WVU)—and the engineering and construction expertise of an industry partner (URS Corporation).

NRAP Technical Leadership Team

Jens Birkholzer
LBNL Technical Coordinator
Lawrence Berkeley National Laboratory
Berkeley, CA

Grant Bromhal
NETL Technical Coordinator
Lead, Reservoir Working Group
Office of Research and Development
National Energy Technology Laboratory
Morgantown, WV

Chris Brown
PNNL Technical Coordinator
Lead, Groundwater Working Group
Pacific Northwest National Laboratory
Richmond, WA

Susan Carroll
LLNL Technical Coordinator
Lawrence Livermore National Laboratory
Livermore, CA

Laura Chiaramonte
Lead, Natural Seals Working Group
Lawrence Livermore National Laboratory
Livermore, CA

Tom Daley
Lead, Monitoring Working Group
Lawrence Berkeley National Laboratory
Berkeley, CA

George Guthrie
Technical Director, NRAP
Office of Research and Development
National Energy Technology Laboratory
Pittsburgh, PA

Rajesh Pawar
LANL Technical Coordinator
Lead, Systems Modeling Working Group
Los Alamos National Laboratory
Los Alamos, NM

Tom Richard
Deputy Technical Director, NRAP
The Pennsylvania State University
NETL-Regional University Alliance
State College, PA

Brian Strazisar
Lead, Wellbore Integrity Working Group
Office of Research and Development
National Energy Technology Laboratory
Pittsburgh, PA

Sean Plasynski
Deputy Director
Strategic Center for Coal
National Energy Technology Laboratory
U.S. Department of Energy

Jared Ciferno
Director
Office of Coal and Power R&D
National Energy Technology Laboratory
U.S. Department of Energy

Robert Romanosky
Technology Manager
Office of Coal and Power R&D
National Energy Technology Laboratory
U.S. Department of Energy

Regis Conrad
Director
Division of Cross-cutting Research
Office of Fossil Energy
U.S. Department of Energy

NRAP Executive Committee

Cynthia Powell
Director
Office of Research and Development
National Energy Technology Laboratory
U.S. Department of Energy

Alain Bonneville
Laboratory Fellow
Pacific Northwest National Laboratory

Donald DePaolo
Associate Laboratory Director
Energy and Environmental Sciences
Lawrence Berkeley National Laboratory

Melissa Fox
Chair, NRAP Executive Committee
Program Manager
Applied Energy Programs
Los Alamos National Laboratory

Julio Friedmann
Chief Energy Technologist
Lawrence Livermore National
Laboratory

George Guthrie
Technical Director, NRAP
Office of Research and Development
National Energy Technology Laboratory

NRAP Technical Report Series